



## Hydrogeological controls on spatial patterns of groundwater discharge in peatlands

Danielle K. Hare<sup>1,2</sup>, David F. Boutt<sup>2</sup>, William P. Clement<sup>2</sup>, Christine E. Hatch<sup>2</sup>,  
5 Glorianna Davenport<sup>3</sup>, Alex Hackman<sup>4</sup>

<sup>1</sup>AECOM Technical Services, Rocky Hill, CT 06067

<sup>2</sup>Department of Geosciences, University of Massachusetts Amherst, 611 N. Pleasant St., Amherst, MA,  
01003, USA

10 <sup>3</sup>Living Observatory at Tidmarsh Farms, 139 Bartlett Road, Plymouth, MA, 02360, USA

<sup>4</sup>Massachusetts Division of Ecological Restoration, 251 Causeway St., Suite 400, Boston, MA 02114

*Correspondence to:* Danielle K. Hare ([hare.danielle@gmail.com](mailto:hare.danielle@gmail.com))



15 **Abstract.** Peatland environments provide important ecosystem services including water and carbon  
storage, nutrient processing and retention, and wildlife habitat. However, these systems and the services  
they provide have been degraded through historical anthropogenic agricultural conversion and dewatering  
practices. Effective wetland restoration requires incorporating site hydrology and understanding  
20 groundwater discharge spatial patterns. Groundwater discharge maintains wetland ecosystems by providing  
relatively stable hydrologic conditions, nutrient inputs, and thermal buffering important for ecological  
structure and function; however, a comprehensive site-specific evaluation is rarely feasible for such  
resource-constrained projects. An improved process-based understanding of groundwater discharge in  
peatlands may help guide ecological restoration design without the need for invasive methodologies and  
detailed site-specific investigation.

25

Here we examine a kettle-pond peatland in southeast Massachusetts historically modified for commercial  
cranberry farming. During the time of our investigation, a large process-based ecological restoration project  
was in the assessment and design phases. To gain insight into the drivers of site hydrology, we evaluated  
the spatial patterning of groundwater discharge and the subsurface structure of peatland complex using  
30 heat-tracing methods and ground penetrating radar. Our results illustrate that two groundwater discharge  
processes contribute to the peatland hydrologic system: diffuse lower-flux marginal matrix seepage; and,  
discrete higher-flux preferential-flow-path seepage. Both types of groundwater discharge develop through  
interactions with subsurface peatland basin structure, often where the basin slope is at a high angle to the  
regional groundwater gradient. These field observations indicate strong correlation between subsurface  
35 structures and surficial groundwater discharge. Understanding these general patterns may allow resource  
managers to more efficiently predict and locate groundwater seepage, confirm these using remote sensing  
technologies, and incorporate this information into restoration design for these critical ecosystems.



## 40 **1 Introduction**

Peatlands develop in response to physical, biological, and chemical processes and feedbacks. Groundwater discharge to surface water is one of the most important physical controls on peatlands stability (Siegel et al., 1995; Watters and Stanley, 2007); yet the underlying physical hydrogeologic framework governing the development of surface seepage distribution in these systems is not well understood. Preferential flow paths, hydraulic conductivity ( $K$ ) anisotropy, and geologic heterogeneities likely influence the surface expression of discharge zones (Chason and Siegel, 1986; Drexler et al., 1999; Smart et al., 2012). However, these variables have been difficult to constrain due to the spatial resolution of traditional localized groundwater wetland methods (wells, boreholes, surface point measurements, etc.), and their impact on fragile flow paths. The underlying hydrologic engine of these wetlands have shown to be difficult to discern on large scale systems.

Thermal dynamics of ground and surface waters also govern critical wetland functions and can be assessed in multiple ways. Surface water thermal stability, for example, is a popular research focus in ecohydrology, as this process is important for aquatic species that rely on the low variance of groundwater temperature to buffer themselves from heat extremes and regulate their metabolism (Caissie, 2006; Deitchman and Loheide II, 2012). Temperature also controls chemical processes in ecosystem respiration, which in turn controls carbon processing and nutrient retention (Boulton et al., 1998; Davidson and Janssens, 2006; Demars et al., 2011; Lafleur et al., 2005), biodiversity (Parish et al., 2008), and overall species health (Verberk et al., 2011). Upwelling zones are increase biogeochemical cycling (Sebestyen and Schneider, 2001), and also maintain species richness through ‘edge effect’- overlap between the thermal and chemically stable groundwater ecotone and the higher oxygen environment within the main stream channel (Brunke and Gonser, 1997; Cirkel et al., 2010). An increase in wetland temperature has been shown to stimulate methane production (McKenzie et al., 2007) as well. The underlying drivers of the thermal regime of a wetland system can be caused through varying driving processes, and are important to the ecosystem services provided in the peatland.

Widespread drainage of peatlands has caused wetland degradation and loss of ecosystem services. Anthropogenic modifications such as ditching and filling create discontinuity between surface water and groundwater systems with impacts to wetland function (van Loon et al., 2009). In some parts of the world, wetland restoration is attempting to address these historical impacts. Within the United Kingdom, for



example, efforts to return natural water table levels by filling drainage ditches in peat mining areas have led to disagreements as to the cost-benefits of these specific restoration designs (Grand-Clement et al., 2013). In New England (United States), where thousands of acres of historical peatlands were converted to commercial cranberry farming in the late 1800s (Garrison and Fitzgerald, 2005), wetland restoration is similarly attempting to regain natural water table levels (Price et al., 2003). An incomplete understanding of underlying hydrology and thermal regime can limit the effectiveness of such efforts.

In this research, we explore the spatial distribution of groundwater seepage through a kettle-hole peatland from the analysis of basin structure and hydraulic properties of the peatland matrix. To help assist in wetland restoration design at our study site, we focus on understanding the natural processes that promote the hydrologic inputs for aquatic habitat formation and maintenance. The goals of this study are to: (1) identify groundwater discharge locations and their hydrogeologic controls, (2) determine temperature dynamics of the groundwater discharge locations, and (3) evaluate the development of these seepage patterns. Through this work, insight is gained into the hydrologic driving mechanisms of peat-based wetlands to help support restoration of sustainable ecosystems (e.g. process-based design) (Beechie et al., 2010; Dahl et al., 2007).

### 1.1 Site Description

The site ‘Tidmarsh Farms’ is consolidated 3 cranberry farms, and the two largest farms (Tidmarsh East and Tidmarsh West) are separated by Beaver Dam Road. All farms were built on kettle hole peatlands between the late 1800’s and early 1900’s. In 2010, the cranberry peatlands on Tidmarsh East were taken out of production; the peatlands on Tidmarsh West were taken out of production in 2015. The current paper concerns work on Tidmarsh East (the Site), which is 2.5 km<sup>2</sup>. Both farms drain into the small 5 km<sup>2</sup> surficial Beaver Dam Brook Watershed, but are also a discharge location of the 360 km<sup>2</sup> Plymouth-Carver-Kingston-Duxbury (PCKD) groundwater aquifer, thus the groundwater flowpaths contribute from a much larger hydrologic system than the surficial watershed (Fig. 1A). The PCKD aquifer surrounding the site is characterized by glacial outwash sands (Masterson et al., 2009), which includes the aquifer underlying the peat. Surface water enters the site from four surface water bodies south of the site (Fresh Pond, Little Island Pond, the Arm Wetland, and Beaver Dam Pond headwaters), and drains northward into Beaver Dam Brook, an approximately 2 kilometer reach, before discharging in Bartlett Pond and then directly into Plymouth Bay (Fig. 1B).



105 Cranberry farming practices had applied 0.3-1.5 meters of locally-mined sand over native surficial soils as of the Site retirement in 2010. To facilitate drainage and irrigation, lateral and perimeter drainage ditches exist throughout farmed areas. Parallel drainage ditches are located approximately every 35 meters throughout the entire site, and are approximately 1 meter wide and 0.5 meter deep. The western agricultural cells have drainage ditches oriented east-west (Cell 3 and 4), and in the eastern cells (Cell 6 and 7) most drainage ditches are oriented north-south).

110 Flashboards in the dam creating the Beaver Dam Pond impoundment were permanently removed by the landowners in the fall of 2010, and since then the southern side of the farm has been allowed to drain and return to a natural wetland state (Fig.1B). Data collection conducted for this research spanned 2012-2014, beginning two years after farming ceased, and prior to any active wetland restoration activity.

115 During this research, which was conducted under collaboration between Living Observatory and University of Massachusetts, a restoration project involving the private landowners, governmental agencies, and non-governmental organizations was in assessment and design phases. Project planners were specifically interested in the location of spring emergence across the site to help guide placement of reconstructed stream channels. In addition, the restoration design team sought to better understand the location of subsurface peat deposits, underlying site hydrology, and potential future thermal regime when considering  
120 potential restoration activities. As of 2017, the site has undergone both passive and active restoration to encourage an accelerated ecological recovery based on the conclusions of this work. In the following sections, we document our methods and finding specific to the spatial distribution of the groundwater discharge at Tidmarsh East and the implications for restoration design.

## 2 Methods

125 Seepage patterns within peatlands have been difficult to constrain due to large site areas and complex, dynamic substrate. At Tidmarsh Farms, we use multiple remote-sensing and direct-contact methods in this environment to connect data from different scales into a process-based understanding of peatland groundwater seepage. Ground penetrating radar (GPR) is used to evaluate the subsurface structure of the peatland basin(s), and multiple thermal methods are used to locate and analyze surficial groundwater  
130 seepage patterns. Stable water isotopes are used to describe dominant water sources supplying the seepage.

Traditional hydrogeologic methods were also implemented including well transects, seepage meters and differential discharge gauging along Beaver Dam Brook. Figure 1A illustrates the location of field



135 measurements. Differential discharge gaging of surface water flow was performed at the site with a Marsh  
McBirney Flo-Mate 2000. Seepage meter measurements were performed using low-profile seepage meters  
designed for use in flowing water (in accordance with technique described by Rosenberry, 2008).

### 2.1 Resolving Subsurface Structure

140 GPR has been successfully used to characterize peatlands' physical structure and stratigraphy due to the  
strong contrast between peat and the underlying aquifer geophysical properties (e.g. water content) (e.g.  
Comas et al., 2005; Holden, 2004; Kettridge et al., 2008; Lowry et al., 2009; Slater and Reeve, 2002). The  
GPR method relies on the transmission of electromagnetic (EM) waves through the subsurface then records  
the time and amplitude of the returning signal (reflection) to image changes in the electromagnetic  
properties between subsurface materials (Knight, 2001; Lowry et al., 2009). We used common-offset  
145 reflection profiling to acquire GPR data with both 100 MHz and 50 MHz antennas with a transmitter-  
receiver separation of 1 meter and 2 meters respectively; however, we only use of the 100 MHz data to  
generate interpolated maps of peat thickness, as that data provided better resolution of the peat-sand  
interface. Nineteen line surveys were completed; all surveys used 0.3-meter trace spacing and ranged from  
100 meters to 1000 meters in total length (Fig. 2).

150 We applied a 150 MHz high-cut filter to remove the high frequency noise, and then a 100 nano-second  
automatic gain control to compensate for signal loss with depth. The peat-sand interface was determined in  
each of the radargrams. Three characteristic radargrams are shown in Figure 2.

155 We constrain the EM signal velocity through the peat for the GPR data analysis, and describe the peat's  
structure with depth by collecting nine sediment cores (Fig. 1B). These cores were collected and analyzed  
from the ground surface to the underlying sand using both vibracore (3) and hand cores (6). We determined  
an average EM velocity of 0.036 m/ns through the peat, which is consistent with other GPR peatland  
research (0.033-0.039 m/ns) (Lowry et al., 2009). Using these data, a 3D interpolation of the peat-sand  
160 interface was created using kriging to estimate the subsurface peat basin structure (Fig. 2). The second  
derivative of the maximum slope (profile curvature) was calculated from the interpolated surface to identify  
changes in basal peat slope change, and is shown in Figure 2.

### 2.2. Identifying locations of groundwater discharge to surface water using temperature

Heat can be used as a tracer to identify upwelling groundwater, as air temperature oscillations on diurnal  
and annual timescales strongly influence surface waters, while deep (e.g. greater than approximately 10 m)



165 groundwater temperatures remain relatively constant through time (Anderson et al., 2005; Constantz,  
1998). Local, shallow flow paths can be more sensitive to climatic and seasonal changes in evaporation and  
precipitation (Fraser et al., 2001; Kurylyk et al., 2014b; Menberg et al., 2014; Reeve et al., 2006), and may  
not contribute to the thermal stability of aquatic systems to the same extent as deep (>10m), regional  
aquifers. This noted, during the thermal study periods groundwater temperatures range from 10-11 °C in  
170 onsite wells below the peat.

### 2.2.1. Fiber-Optic Distributed Temperature Sensing

Raman spectra fiber-optic distributed temperature sensing (FO-DTS) is used for spatially extensive heat  
tracing in aquatic systems. Tyler et al., 2009 provides a thorough review of the details of the technology  
and calibration. DTS temperature data were collected with Sensor Tran Gemini HT control unit in dual-  
175 ended mode on AFL telecommunications umbilical cable. This FO-DTS unit allows for 1-meter spatial  
accuracy at 0.1°C precision over ~15 min integration times. Each FO-DTS deployment was operated for a  
minimum of 5 days to ensure multiple sufficiently strong diurnal signals were captured. Fifty-meter  
calibration coils were maintained at a constant temperature with an ice-water slush bath and/or ambient  
bath and were compared to an independent Onset HOBO Water Temperature Pro v2 Data Logger (U22-  
180 001) ( $\pm 0.2$  °C accuracy).

In July and August of 2013 four FO-DTS deployments were installed, one within the drainage ditches of  
eastern peatland cells, and three within the western cells. We capitalize on the modified structure of the  
agricultural peatland surface, particularly the relatively evenly spaced drainage ditches, to thermally sample  
185 surface water in a distributed way which is not possible in more natural systems (e.g. Lowry et al., 2007).  
The deployment sites were chosen based on previous infrared surveys (November 27<sup>st</sup>, 2012, discussed in  
Sect. 2.2.2), interviews with the previous farmer, and feasibility of installation. Each deployment ranged  
from 1000m-2500m in length. Macrophyte growth was cleared during installation and continuously  
monitored through each deployment.

190 FO-DTS data analysis consisted of mean and standard deviation calculations on the ~5-day time series at  
every 1-m along the cable to identify locations of groundwater seepage and indicate its relative magnitude  
and permanence, which is not possible for other “snapshot” in time methods (Briggs et al., 2012; Hare et  
al., 2015; Sebok et al., 2013; Selker et al., 2006).



195 **2.2.2. Infrared Surveys**

Thermal infrared (TIR) cameras sense and quantify surface infrared (heat) radiation, and are increasingly being used to evaluate aquatic systems efficiently at large scales (Chen et al., 2009; Deitchman and Loheide, 2009; Dugdale et al., 2016; Handcock et al., 2012; Hare et al., 2015), particularly at large sites, or sites where in-situ measurements are not possible. The hand-held TIR survey was conducted to both  
200 expand the thermal survey and to compare this method to the FO-DTS data. We used a high-resolution forward-looking infrared camera (T640BX model FLIR, FLIR Systems, Inc.) with GPS and compass capabilities. The TIR method allowed for efficient spatial coverage, and allowed us to obtain thermal data unreachable with FO-DTS (Hare et al., 2015).

205 At Tidmarsh Farms East three TIR surveys were completed: July 30-31<sup>st</sup>, 2013; March 21, 2014; and one reconnaissance survey on November 27<sup>th</sup>, 2012. The July survey was used to make comparisons to the FO-DTS data as it was taken during the same time period; the March survey was used to compare seasonal variability in seepage patterns. To create a spatial site map comprised of all TIR images, a single temperature (color-contoured pixel) from an aquatic point of interest was selected, and used to color an  
210 icon on the map. This allowed for georeferenced IR data to be used quantitatively to evaluate seepage patterns by location. The relative magnitude of seepage rate is estimated based how similar the observed temperature is to the regional groundwater temperature.

**2.2.3. One-Dimensional Vertical Temperature Profiles**

The depth to which the surface diurnal temperature signal penetrates saturated near-surface sediments  
215 depends on the period of the signal, the fluid flow velocity and direction, and the physical properties of the fluid-saturated sediment (Goto et al., 2005; Hatch et al., 2006; Irvine et al., 2016; Stallman, 1965). With depth, the diurnal heat signal variation decreases in amplitude and its shifts forward in time. Much of the heat transport not explained by pure conduction is attributable to advective fluxes, which can be solved for from thermal time-series at multiple depths using simple analytical solutions to the one dimensional heat  
220 transport equation with specified boundary conditions (Hatch et al., 2006; Rau et al., 2014; Schmidt et al., 2007; Silliman et al., 1995; Stallman, 1965).

We analyzed four 1D vertical temperature profiles to understand the vertical subsurface fluid flux patterns at the site. Maxim iButtons temperature loggers (0.0625 °C resolution; 1°C accuracy model #) were  
225 attached to cavities drilled into a wooden dowel, and placed into the ground such that their located at -2.5, -5.0, -10.0, -25.0 cm depth and one at +2.5 cm above the surface. We coated each iButton with silicon





sealant to prevent leaking/sensor damage; however, a 25% sensor failure rate was still experienced. A 10-minute sampling interval was used for a minimum of 7 days during July and August of 2013 for each temperature time series.

230

Installation locations chosen represented the two types of seepage observed with the FO-DTS, and 1D vertical temperature data were collected synchronously with DTS deployments. Two additional control deployments of 1D temperature profiles were installed within/below drainage ditches. We assume that under low surficial flow conditions the system is at quasi-steady-state, allowing us to estimate (upward) seepage flux from measured surface water, groundwater, and intermediate-depth temperatures using the analytical solution to the heat transport equation derived by Turcotte and Schubert (1982) and modified by Schmidt et al. (2007).

235

### 2.3 Assessment of environmental isotopes to infer groundwater flow paths

To trace the source of the groundwater flow paths contributing to discharge, we use  $\delta^{18}\text{O}$  and  $\delta^2\text{H}$  to distinguish between local recharge (short flow paths) and regional recharge (long flow paths). The isotopic composition ( $\delta^2\text{H}\text{-H}_2\text{O}$ ,  $\delta^{18}\text{O}\text{-H}_2\text{O}$ ) of hydrogen and oxygen of the water molecule was analyzed for water samples collected from surface water (monthly), shallow ground water (seasonally), deep groundwater (seasonally), groundwater seepage (August 2013) and pore waters (October 2013). Upper 1-meter peat pore water samples were acquired through a manual press of samples from Russian peat cores, and subsequently filtered for analysis.

240

245

$\delta^2\text{H}\text{-H}_2\text{O}$  and  $\delta^{18}\text{O}\text{-H}_2\text{O}$  was measured by wavelength scanned cavity ring-down spectrometry on unacidified samples with a Picarro L-1102i WS-CRDS analyzer (Picarro, Sunnyvale, CA). Samples were vaporized at 110°C. International reference standards (IAEA, Vienna, Austria) were used to calibrate the instrument to the VSMOW-VSLAP scale and working standards were used with each analytical run. Three standards that isotopically bracket the sample values are run alternately with the samples. Secondary laboratory reference waters (from Boulder, Colorado; Tallahassee, Florida; and Amherst, Massachusetts) were calibrated with Greenland Ice Sheet Precipitation (GISP), Standard Light Antarctic Precipitation (SLAP) and Vienna Standard Mean Ocean Water (VSMOW) from the IAEA. Results are calculated based on a rolling calibration so that each sample is determined by the three standards run closest in time to that of the sample. Long-term averages of internal laboratory standard analytical results yield an instrumental precision of 0.51 ‰ for  $\delta^2\text{H}\text{-H}_2\text{O}$  and 0.08 ‰ for  $\delta^{18}\text{O}\text{-H}_2\text{O}$ .

250

255



260 The USGS wells were sampled for groundwater isotopic compositions within the PCKD aquifer, providing regional groundwater values for the aquifer and defining the expected annual range of isotopic values for local precipitation (Table 1). The regional groundwater trend line was generated by fitting a linear regression through the USGS well isotope data from regional PCKD aquifer.

#### 4 Results

265 As an initial evaluation of the groundwater contribution to the site, we conducted differential discharge gauging measurements. The stream gained  $6 \text{ L s}^{-1}$  discharge through Cell 7 from Arm Pond input to the confluence with Beaver Dam Brook (1.5 km), equal to an average of  $0.004 \text{ L s}^{-1}$  per meter of river length (Fig. 1B). Cell 3 and 4 gained  $113 \text{ L s}^{-1}$  from the Beaver Dam Pond input to the confluence with East side river (1 km), equal to an average of  $0.113 \text{ L s}^{-1}$  per meter of river length.

##### 4.1 Resolving Peatland Basin Structure

270 The interpolation of the basal surface, or the peat-sand contact beneath the peat from GPR data indicates four isolated peat depressions at the site, two depressions in Cell 6 and Cell 7 and two Cell 3 and Cell 4. The Cell 6 and 7 have a maximum peat thickness of  $\sim 7$  meters and a gradual curvature of the peat/sand contact than the western cells, Cell 3 and Cell 4 (Fig. 2). The western cells show a maximum peat thickness of  $\sim 10$  meters, and high curvature values. The basin structure of the western cells is also more complex  
275 than Cell 6 and 7, as Cell 3 and Cell 4 have pronounced undulations in the basal peat-sand contact surface, creating dramatic changes in basin shape. Particularly, there is a notably high curvature of the basal peat/sand contact along the western edge approximately 30 meters from the margin. The GPR profiles illustrate multiple series of normal faults beneath the peat body that are consistent with ice melt-out and/or collapse features (Fig. 2) typical of kettle pond origin (Kruger et al., 2009).

##### 280 4.2 Thermal evaluation of groundwater seepage

Surface water temperatures in the main channel and ambient drainage ditch environments generally show high standard deviation, indicative of a coupling between these surface waters and air temperatures, and mean water temperatures closely tied to the seasonal surface temperature average, also indicative of surface water dominance. TIR and FO-DTS surveys were designed to detect low standard deviation and consistent  
285 mean temperature anomalies from these background conditions, which would be indicative of groundwater inflows. An alternative explanation for this low variance could be coverage via mobile sediment (Sebok et al., 2015); however, within this peatland environment this process is not expected, nor was observed. The



temperature results of both these surveys are presented in Hare et al. (2015). Results from both TIR and FO-DTS identified two categories of thermal anomalies: type 1 anomalies manifest as temperatures with relatively low standard deviation through time, and an anomalous heat signature that is approximately regional groundwater temperature  $\pm 3\text{-}5$  °C; and type 2 thermal anomalies also have a low standard deviation, but temperatures more closely resemble regional groundwater temperatures (10-11 °C). Figure 3 shows time series data collected with the FO-DTS and illustrates each of the major thermal signatures shown on site: temperatures of groundwater, the main channel, a drainage ditch, and the two thermal anomalies. We interpret these two anomalies to correspond to two modes of seepage, type 1 thermal anomalies correspond to matrix seepage, and type 2 thermal anomalies correspond to preferential flow path (PFP) seepage. The two seepage types are clearly differentiated through thermal signatures, and can be isolated using the average and standard deviation of temperatures with time. The TIR surveys supported and reinforced these two distinct types of seepage, which were present in both the summer and winter surveys (Fig. 4).

TIR surveys and FO-DTS data indicate that most groundwater-influenced temperature occurs along the western edge of the Cell 3 and Cell 4, where peat is thinner or where there is strong sand/peat contact curvature in peat basin shape (Fig. 5). Consistent temperatures similar to groundwater temperatures and anomalously low standard deviations exist along the linear location of highest peat/sand contact curvature near the western edge of the cells temperature analysis yields a number of isolated locations. These isolated, unique locations of type 2 seepage occurring within the deeper peat represent a distinct seepage process from type 1 seepage.

During the March infrared survey, a high density of ~1-5 cm diameter flowing macropores within the peat was discovered on the interior of the Cell 3. The water discharging from these macropores exhibited typical type 2 seepage temperatures (Fig. 6), and led us to term this mode of PFP seepage. This observation is similar to the peat macropores or ‘peat pipes’ described in previous peatland research (e.g. Briggs et al., 2016; Cunliffe et al., 2013; Holden, 2004; Smart et al., 2012; Vandenbohede et al., 2014), but the concentration of macropores in this singular location makes the northwest cell macropores observation unique. Due to the high flux observed from PFP seeps, even though the quantity is small, these PFPs have the potential to contribute significantly to the groundwater gain at sites (Poulsen et al., 2015). The peat thickness map (Fig. 5) indicates that the zone of high macropore density is an area of peat thinning reaching a minimum peat thickness of 3 m, and also a location of high curvature (center of cell 3). Rossi et al. (2012) describes similar correlation to peat thinning at their site in Finland.



### 4.3 1D vertical temperature profiles

The two seepage types and two ambient drainage ditch locations were monitored with 1D vertical temperature profiles for seven to ten days. We expected to observe significant upwelling at this site, which we could easily identify by a rapid attenuation of the diurnal signal with depth coupled with a characteristic convex shape of mean temperature with depth (Schmidt et al., 2007). Temperatures from all four 1D vertical temperature profiles are distinct from one another; however, all the temperature profiles, including the “ambient” drainage ditches, indicate upwelling of groundwater (convex shape of mean temperature with depth in Fig.7). The surface temperature of the ambient drainage ditches (temperature profiles 3 and 4) is similar to the diurnal temperature cycles measured with FO-DTS. As water was shallow in most ditches (<0.5m) with no thermally significant influx of groundwater, water in and below the ditch was expected to have temperatures similar to, or warmer than air temperature. However, the subsurface profiler results show a characteristic upwelling thermal envelope (convex shape); except the entire temperature envelope is 7-10 °C warmer than average groundwater. In addition, the mean temperature at depth this time of year is 13-15 °C at -25 cm, significantly warmer than the groundwater temperature. Using these temperature time series to solve for 1D upward fluid flux yielded -0.11 and -0.20 m d<sup>-1</sup> for these drainage ditches. These flux values are similar to the seepage observed at temperature profiler 1. Despite our intention to use these locations as control points for pure-conduction temperature-depth profiles, upwelling was observed beneath the ditches as well.

325

330

335

340

345

350

Temperature profiler 1 was installed at a location with a surficial temperature of 13-14 °C in August 2013. The total peat thickness at this location is 50 cm, and consistent with groundwater upwelling, minimal diurnal signal propagates to depth, and surface water exhibits relatively low variance in temperatures over time. Thermal time series estimates of flux show a modest -0.23 m d<sup>-1</sup> upwelling through the peat at this seepage location.

Finally, temperature profiler 2 was installed in a location with a surficial temperature consistent with groundwater temperatures of 10-11 °C in August 2013, and temperatures with depth exhibit a groundwater thermal signal throughout the entire profile. Even close to the bed interface, the streambed thermistor (2.5 cm) shows slight thermal shifts ( $\sigma = 0.096$  °C), which are near to the resolution of the instrument (0.0625 °C). This unique temperature profile is indicative of high upward flux rates, as the diurnal signal cannot be resolved and there is essentially no downward conduction from above; therefore, we were unable to use the steady state analytical solution to estimate a flux rate. However, in July 2015, we deployed a seepage meter



at this location and measured fluxes in excess of  $3 \text{ m d}^{-1}$ , rates which exceed the limits for analytical flux calculations.

#### 355 **4.4 Groundwater Discharge Source Areas**

Groundwater discharge to the wetland complex is a mixture of shallow and deep regional flow paths. Isotopic analyses of waters from wells in the up-gradient portion of the PCKD aquifer (blue circles in Figure 8) fall along a regional groundwater trend line. We interpret this regional trend line to be characteristic of the annual isotopic composition of recharge water to the region as well as local groundwater recharge in the topographic watershed of Tidmarsh. This water isotopic values plot left of the global meteoric water line (GMWL)(Craig, 1961), which reflects local and regional vapor recycling and a characteristic mixture of vapor sources (Koster et al., 1993). The one exception to this line is the USGS well MA-PWW 494 in Plymouth, MA which is similar to Tidmarsh in that it is downgradient of the recharge area of the PCKD aquifer. This water falls to the right of the regional groundwater trend line. Discharging and shallow groundwaters at the wetland site plot close to but off of the regional groundwater trend line. The blue diamonds (Fig. 8) represent a monthly sampling of wetland surface waters that depict a significant clustering to the right of the regional groundwater trend and evolve along a line tangent to this intersecting the deep TM groundwater. Uncharacteristically, the deepest sampled groundwater at the site ( $>15 \text{ m}$ ) falls even to the right of the GMWL, suggesting this water has experienced a significant enrichment in the heavy isotopes due to evaporation processes. Repeated sampling of this water reveals a consistent isotopic composition that suggests the deep groundwater beneath Tidmarsh is isotopically enriched due to evaporation from open water bodies in upgradient kettle ponds. Headwater seepage and a repeatedly sampled of strong discharge (large pink and red triangles in Figure 8) in the interior of the wetland complex fall along a line that represents either a mixture of this evaporated water and the regional groundwater trend (finely dashed line) or itself is simply an evaporatively evolved water. Both interpretations suggest that the source of water to the shallow groundwater wells and the large volume springs in the interior of the wetland complex are distinct. This indicates that the local flow path from the southwest to the northeast is the large-scale hydraulic gradient that dominates the observed seepage patterns. The orientation of peatland basin slope break and the regional groundwater gradient also intercept the southwest corner of the peatland where numerous high-flux groundwater seeps are located.



## 5 Discussion

### 5.1 Groundwater discharge types

Two types of groundwater discharge (or seepage) were identified using thermal methods. First, discharge areas that have regional groundwater temperature (e.g. 10-11 °C). Second, seepage locations with  
385 temperatures that are offset ( $\pm 3$ -5°C) from groundwater temperature, but have very low variance and are also significantly distinct from local surface water temperatures. Both seepage types appear to strongly buffer stream temperatures, illustrated by low variance when examined through time (FO-DTS data). The identification of these two distinct seepage types using multiple methods and during distinct seasons indicates different mechanisms for generation of each of these seepage patterns. Figure 5 combines these  
390 two types of seepage observed with either FO-DTS or TIR to evaluate spatial patterning and consistencies, and shows how the two types are related to one another as well as to patterns of high basal curvature.

Consistent (low standard deviation) and groundwater-like temperatures (10-11°C) of the type 2 seepage indicate very high flux ( $>3 \text{ m d}^{-1}$  was confirmed with seepage meter measurements). Given the low vertical  
395 K of peat matrices, sustaining such high fluxes would require seemingly implausible hydraulic gradients, certainly far above the vertical hydraulic gradients observed on site. Therefore, it is highly likely that this seepage does not occur through the peat media/ matrix itself, but instead consistent with “short-circuit discharges” described by Conant Jr. (2004). Focused flow in conduits through the peat was observed in the field at Tidmarsh Farms (Fig. 6), and by Briggs et al. (2016), and has been documented through visual descriptions of peat pipes, or macropores at other locations (Baird, 1997; Beckwith et al., 2003; Cunliffe et al.,  
400 2013; Holden, 2004; Smart et al., 2012; Wallage and Holden, 2011). However, the spatial extent of these preferential flow zones has not been previously demonstrated. Due to their high flux, physical isolation, and focused nature, we refer to this type of seepage as preferential flow path (PFP) seeps in the following discussion.

405 Data represented by type 1 seepage show that surface water diurnal temperatures are also buffered in these zones and are distinct from most ambient surface temperatures. This observation could indicate shallow aquifer groundwater discharge, which is more influenced by atmospheric temperatures than deeper regional flow (Kurylyk et al., 2014a; Menberg et al., 2014). However, consistent temperatures in the site’s shallow groundwater wells and 1D temperature profiles indicate that these seepage temperatures are controlled by a  
410 lower flux rather than distinct atmospheric-influenced shallow flow paths. These type 1 seeps indicate that while vertical upwelling fluxes are present, they are much smaller than PFP discharge zones, and must be controlled by a different mechanism. Thermal profilers yielded vertical flux rates consistent with a low to



415 moderate upwelling through porous media according to *Conant Jr. (2004)*; which would be typical of the hydraulic properties associated with peat, and thus, we refer to locations with this signature as “matrix” seeps. The two seepage types, PFP and Matrix seepage, are similar to the “point” and “diffuse” peat seepage categories defined by *Rossi et al. (2012)*, but rather than focusing on the area of influence, instead highlight the physical structure that governs the process which ultimately generates seepage in these peatland seepage zones.

420 Within the drainage ditches that have no thermal indication of groundwater discharge, a vertical flux was nevertheless present at a magnitude similar to matrix seep flux. This was observed in both temperature profiles 3 and 4 (Fig. 7). A longer flow path within the peat’s catotelm may explain the similar vertical flux rates to matrix seepage, but with a warmer surface expression. This indicates upwelling throughout the entire site; though these locations do not appear to contribute to the thermal buffering of the surface waters.

## 5.2 Subsurface Structural Control on the Spatial Distribution of Seepage Types

425 Matrix seeps were plentiful within approximately 30 m of the peatland edge (Fig. 5), consistent with margin seepage observed in lake environments (*Rosenberry et al., 2010; Sebestyen and Schneider, 2004; Sebok et al., 2013; Winter, 2001*) and other wetlands (*Freeze, 1988; Labaugh et al., 1998*). The peat is 0.1-3.0 meters thick along the margin where matrix seepage occurs (Fig. 3), which is generally significantly thinner than locations of observed PFP seepage. Matrix seeps generally occur in the thinnest peat zones, and typically decrease rapidly with distance from the peatland edge toward the interior slope change, after which no thermally distinct groundwater discharge points are observed (Fig. 5). Similar landscape-scale observations have been made within lakes and wetlands (e.g. *Cherkauer and Zager, 1989; Sebok et al., 2013*), and as kettle hole peatlands typically form from initially open water bodies, there are logical similarities in basic processes between the two environments.

435 Discrete seepage zones may reflect zones of higher effective  $K$  than the surrounding peat matrix, which could be explained by littoral-zone migration in the lake to wetland evolution as the water table fluctuates and migrates. In lake environments, diffuse matrix seepage occurs because of an increase in  $K$  at the edge of the lake caused by “erosional deposition,” whereby focused wave and current action disrupt and erode sediments, particularly mobilizing the finest sediments elsewhere, and concentrating larger particles, indicative of these higher-energy environments in these locations. Preferentially stronger flow paths are thus concentrated at the break in land surface slope (*Blume et al., 2013; Casson et al., 2010; Cherkauer and McKereghan, 1991; McBride and Pfannkuch, 1975; Rosenberry et al., 2010; Winter, 1981*). Previous work



445 propose that seepage flux decreases exponentially with distance from shore of a lake (Cherkauer and Zager, 1989; McBride and Pfannkuch, 1975), which is qualitatively confirmed by our data. Paleoclimate reconstructions have demonstrated that the regional water table around Tidmarsh has been increasing in elevation since the Laurentide ice sheet retreated ~10 ka ago, with 2-3 significant low stands (Newby et al., 2000, 2009). Therefore, we hypothesize that the extent of the matrix seepage observed along the western edge of the peatland is a result of this lake transgression and coincident decrease in deposition of organic material. Here the lower K of the peat matrix intersects with shallow groundwater flowpaths, strongly affecting lateral hydraulic gradients and driving upward flux; a process which likely generates much of the observed matrix seepage. Figure 9 provides a conceptual model of this process, and is supported by similar seepage processes observed in riverine systems (Sophocleous, 2002), wetland (Larsen et al., 2007), lake (Bakker and Anderson, 2002; Winter, 1981) and hillslope environments (Shaw et al., 2017; Winter et al., 1998).

455 In contrast to the matrix seepage, PFP seepage was less common and spatially disconnected from similar flux seeps (Fig. 5). Similar to matrix seepage, PFP seepage exhibits low standard deviation of temperature (Fig. 3), but PFP seep temperatures were much closer to average regional groundwater temperature. This indicates that PFP seepage waters have very short residence times within peatland sediments, which may have important implications for nutrient transformations within them. At PFP seeps peat is generally thicker and located more toward the interior of the peatland rather than along the margin where matrix seepage zones are found (Fig. 5). Typical PFP flow path lengths from the sandy aquifer below the peat to the surface should be much greater than for matrix seeps. However, the thermal signature seems to contradict this. PFP seepage zones must therefore be generated through a unique hydraulic process from matrix seeps. Since PFP seeps at Tidmarsh Farms correlate with significant slope changes, or locations of high curvature, these isolated seepage zones must be generated by an abrupt change in K.

470 An abrupt change from high to low K has long been known to promote the transition from horizontal to vertical flow (Freeze and Witherspoon, 1967). Lowry et al., (2009) hypothesized this process to explain developed seepage within the interior of a peatland through using 3D numerical groundwater flow models. As horizontally flowing regional groundwater encounters a low-conductivity peatland, it is forced to go through or around it, causing pressure to increase where the abrupt change in the K from the sand to catotelm peat matrix occurs. PFP's develop as a fast-pathway to the surface, a pressure-relief valve, where these localized increases in aquifer pressure at the base of the peat matrix translate into strong, sustained discharge of unaltered regional groundwater to the surface.





Rosenberry et al. (2010) notes that in lakes, a significant upward seepage velocity can maintain a locally  
475 high  $K$  as the upward force may suspend smaller particles within the water column. Particulate organic  
matter and lacustrine sediment have a very low settling velocity, therefore if the upward force that  
groundwater seepage induces is greater than the settling velocity, only organic matter with a high mass will  
be able to accumulate over these lake seepage locations. This would cause the peat matrix to have a  
relatively high porosity and a high permeability compared to its surrounding very low permeability matrix.  
480 These locations will continue to be zones of weakness through the formation of the peatland. Thus, we  
hypothesize that high-flux PFP seepage zones persist through the transition from lake to peatland  
environment due to the inability of fine sediments and organic matter to accumulate over these high flux  
locations. Still, these locations of consistently high hydraulic gradient will also continually take advantage  
of inherent matrix weaknesses, such as varying degrees of humification caused by vegetative difference and  
485 water level, or other disruptions in the peat matrix including plant rooting and desiccation ‘cracks’ as  
proposed by (Smart et al., 2012). However, the underlying mechanics of PFP seepage are caused by the  
interception of the regional groundwater gradient and high curvature peat subsurface structure.

The orientation of peatland basin slope break (high basin profile curvature) and the southwest to northeast  
regional groundwater gradient dictates the observed pattern of strong seepage along the western boundary,  
490 which is supported by isotopic analysis. PFP and matrix seep waters both exhibit isotopic signatures  
consistent with a mixture of local groundwater and regional recharge signature (Fig. 8). This observation is  
further reinforced by the increase in net groundwater gain through the western cells, as well as a large  
number of PFP seeps in the southwestern portion of the site (Fig. 5).

## 6 Conclusion

495 Subsurface basin shape exhibits significant control on the spatial distribution of groundwater discharge  
within peatland environments. As horizontal groundwater flow intercepts the peat matrix, two types of  
seepage develop: matrix and preferential flow path seepage. Matrix seepage is defined by a low standard  
deviation in temperature and surface temperature similar to groundwater  $\pm 3-5$  °C, consistent with relatively  
low-flux seepage. Low fluxes are produced where the regional groundwater flow paths intercept the low- $K$   
500 peat at the basin ‘shoreline’, inducing upward flow through relatively thin (0.1-3.0 meters) peat. The  
second type of observed discharge, PFP seepage, has a surface temperatures essentially indistinguishable  
from deep regional groundwater temperature. This indicates very strong upwelling fluxes at these locations  
and little time for conductive heat losses/gains. Locations of PFP seeps correlate with high rates of basal  
peat slope change (curvature) of the peat basin. These seeps develop where the regional groundwater flow



505 path intercepts a secondary slope change and where there is a stark change in K between the high-K sand  
aquifer material and the low-K peat. Together, these physical features generate large pressures, induce  
localized zones of high vertical hydraulic gradient and drive large seepage fluxes upward. Because PFP  
seeps occur typically in locations with thicker peat and yet maintain close to groundwater temperatures,  
they must have a much higher vertical hydraulic gradient and/or higher effective K than the matrix seeps.  
510 Through multiple lines of evidence, we conclude that the development and spatial distribution of  
mineral-tropic peatland seepage is strongly controlled by the interaction between the subsurface basin  
structure, physical process within the peat structure and hydraulic gradient.

Through our results, we establish a predictable pattern of seepage, consistent across the coastal site that is  
515 explained by knowledge of basin shape and regional hydraulic gradient. This information provides  
valuable insight for water resource managers to better understand the natural forces driving groundwater  
seepage. This knowledge, in turn, may be used in the restoration design of degraded peatland systems.  
Knowing where seepage is expected to occur naturally across a site allows for the development of more  
sustainable restoration designs that work with the land, and not against it. In retired cranberry farms, for  
520 example, channels may be relocated to intercept springs to maintain cooler water temperatures. This  
knowledge can also guide the location of targeted intensive grading. For example, as was done at Tidmarsh  
Farms, the dense cranberry mat can be broken up mechanically to encourage groundwater expression on  
former dry farm surfaces and access native seed banks below. Incorporating this data into a restoration  
design will greatly aid the ability to predict and achieve desired ecosystem outcomes, making restoration  
525 projects more efficient, both ecologically and monetarily.

This research provides a process-based investigation of the subsurface hydrodynamics within a peatland.  
While a peat matrix exhibit strongly heterogeneous and anisotropic tendencies, large-scale patterns occur  
and can be predicted. These patterns are dependent on basin shape, peat accumulation history, and  
530 underlying aquifer flow paths. The importance of groundwater flow paths surrounding the peatland and  
resulting seepage patterns emphasizes that peatlands are not isolated entities from the groundwater system  
and cannot be treated as such. Observed large-scale seepage patterning provides insight that may help  
explain vegetation patterning, macropore development, and other localized peat dynamics that have been  
unidentified in the past, and greatly aid peatland management and restoration to establish more naturally  
535 sustainable, efficient practices.



### Disclaimer

The views and opinions expressed in this article are those of the authors and do not necessarily reflect the official policy or position of AECOM Technical Services.

### Acknowledgments

540 This research would like to acknowledge the support of Evan Shulman for site access, field support and his  
humor, Henry Eshbaugh, Eric Van Dam, Steve Hurley and the many volunteers who support the data  
collection efforts site co-ordination. Much gratitude is given to John Lane and Martin Briggs of the U.S.  
Geological Survey, Branch of Hydrogeophysics for equipment rental and technical support. Also, we thank  
Jon Woodruff of the University of Massachusetts, Amherst for use of his laboratory's equipment, data  
545 processing software, student support and technical guidance.

### References

- Anderson, J. K., Wondzell, S. M., Gooseff, M. N. and Haggerty, R.: Patterns in stream longitudinal profiles  
and implications for hyporheic exchange flow at the H.J. Andrews Experimental Forest, Oregon, USA,  
Hydrological Processes, 19(15), 2931–2949, 2005.
- 550 Baird, A. J.: Field estimation of macropore functioning and surface hydraulic conductivity in a fen peat,  
Hydrological Processes, 11, 287–295, 1997.
- Bakker, M. and Anderson, E. I.: Comment on “Numerical investigation of lake bed seepage patterns:  
555 effects of porous medium and lake properties” by Genereux, D., and Bandopadhyay, I., 2001. Journal of  
Hydrology 241, 286–303, Journal of Hydrology, 258(1–4), 260–264, doi:10.1016/S0022-1694(01)00570-4,  
2002.
- Beckwith, C. W., Baird, A. J. and Heathwaite, A. L.: Anisotropy and depth-related heterogeneity of  
560 hydraulic conductivity in a bog peat. II: modelling the effects on groundwater flow, Hydrological  
Processes, 17(1), 89–101, doi:10.1002/hyp.1116, 2003.
- Beechie, T. J., Sear, D. A., Olden, J. D., Pess, G. R., Buffington, J. M., Moir, H., Roni, P. and Pollock, M.  
M.: Process-based principles for restoring river ecosystems, BioScience, 60(3), 209–222,  
565 doi:10.1525/bio.2010.60.3.7, 2010.



- Blume, T., Krause, S., Meinikmann, K. and Lewandowski, J.: Upscaling lacustrine groundwater discharge rates by fiber-optic distributed temperature sensing, *Water Resources Research*, 49, 7929–7944, doi:10.1002/2012WR013215, 2013.
- 570
- Boulton, A. J., Findlay, S., Marmonier, P., Stanley, E. H. and Valett, H. M.: The functional significance of the hyporheic zone in streams and rivers, *Annual Review of Ecology and Systematics*, 29, 59–81, 1998.
- Briggs, M. A., Lutz, L. K., McKenzie, J. M., Gordon, R. P. and Hare, D. K.: Using high-resolution distributed temperature sensing to quantify spatial and temporal variability in vertical hyporheic flux, *Water Resources Research*, 48(2), 1–17, doi:10.1029/2011WR011227, 2012.
- 575
- Briggs, M. A., Hare, D. K., Boutt, D. F., Davenport, G. and Lane, J. W.: Thermal infrared video details multiscale groundwater discharge to surface water through macropores and peat pipes, *Hydrological Processes*, 30(14), 2510–2511, doi:10.1002/hyp.10722, 2016.
- 580
- Brunke, M. and Gonser, T.: The ecological significance of exchange processes between rivers and groundwater, *Freshwater Biology*, 37(1), 1–33, 1997.
- 585
- Caissie, D.: The thermal regime of rivers: a review, *Freshwater Biology*, 51(8), 1389–1406, doi:10.1111/j.1365-2427.2006.01597.x, 2006.
- Casson, N. J., Eimers, M. C. and Buttle, J. M.: The contribution of rain-on-snow events to nitrate export in the forested landscape of south-central Ontario, Canada, *Hydrological Processes*, 24(14), 1985–1993, doi:10.1002/Hyp.7692, 2010.
- 590
- Chason, D. B. and Siegel, D. I.: Hydraulic conductivity and related physical properties of peat, Lost River peatland, northern Minnesota, *Soil Science*, 142(2), 91–101, 1986.
- 595
- Chen, X. H., Song, J. X., Cheng, C., Wang, D. M. and Lackey, S. O.: A new method for mapping variability in vertical seepage flux in streambeds, *Hydrogeology Journal*, 17(3), 519–525, doi:10.1007/S10040-008-0384-0, 2009.



- 600 Cherkauer, D. S. and McKereghan, P. F.: Ground-water discharge to lakes: focusing in embayments, *Ground Water*, 29(1), 72–80, 1991.
- Cherkauer, D. S. and Zager, J. P.: Groundwater interaction with a kettle-hole lake: relation of observations to digital simulations, *Journal of Hydrology*, 109(1–2), 167–184, doi:10.1016/0022-1694(89)90013-9, 1989.
- 605 Cirkel, D. G., Witte, J. M. and van der Zee, S. E. A. T. M.: Estimating seepage intensities from groundwater level time series by inverse modelling: A sensitivity analysis on wet meadow scenarios, *Journal of Hydrology*, 385(1–4), 132–142, doi:10.1016/j.jhydrol.2010.02.009, 2010.
- 610 Comas, X., Slater, L. and Reeve, A.: Stratigraphic controls on pool formation in a domed bog inferred from ground penetrating radar (GPR), *Journal of Hydrology*, 315(1–4), 40–51, doi:10.1016/j.jhydrol.2005.04.020, 2005.
- Conant Jr, B.: Delineating and Quantifying Ground Water Discharge Zones Using Streambed Temperatures, *Ground Water*, 42(2), 243–257, doi:Cited By (since 1996) 93Export Date 4 April 2012, 2004.
- Constantz, J.: Interaction between stream temperature, streamflow, and groundwater exchanges in Alpine streams, *Water Resources Research*, 34(7), 1609–1615, 1998.
- 620 Craig, H.: Isotopic Variations in Meteoric Waters, *Science*, 133(3465), 1702–1703, doi:10.1126/science.133.3465.1702, 1961.
- Cunliffe, A. M., Baird, A. J. and Holden, J.: Hydrological hotspots in blanket peatlands: Spatial variation in peat permeability around a natural soil pipe, *Water Resources Research*, 49(9), 5342–5354, doi:10.1002/wrcr.20435, 2013.
- 625 Dahl, M., Nilsson, B., Langhoff, J. H. and Refsgaard, J. C.: Review of classification systems and new multi-scale typology of groundwater – surface water interaction, *Journal of Hydrology*, 344, 1–16, doi:10.1016/j.jhydrol.2007.06.027, 2007.
- 630



- Davidson, E. A. and Janssens, I. A.: Temperature sensitivity of soil carbon decomposition and feedbacks to climate change., *Nature*, 440(7081), 165–73, doi:10.1038/nature04514, 2006.
- 635 Deitchman, R. and Loheide II, S. P.: Sensitivity of Thermal Habitat of a Trout Stream to Potential Climate Change, Wisconsin, United States, *Journal of American Water Resources Association*, 48(6), 1091–1103, doi:10.1111/j.1752-1688.2012.00673.x, 2012.
- Deitchman, R. S. and Loheide, S. P.: Ground-based thermal imaging of groundwater flow processes at the seepage face, *Geophysical Research Letters*, 36(14), L14401, doi:10.1029/2009GL038103, 2009.
- 640 Demars, B. O. L., Russell Manson, J., Ólafsson, J. S., Gíslason, G. M., Gudmundsdóttir, R., Woodward, G., Reiss, J., Pichler, D. E., Rasmussen, J. J. and Friberg, N.: Temperature and the metabolic balance of streams, *Freshwater Biology*, 56(6), 1106–1121, doi:10.1111/j.1365-2427.2010.02554.x, 2011.
- 645 Drexler, J. Z., Bedford, B. L., Scognamiglio, R. and Siegel, D. I.: Fine-scale characteristics of groundwater flow in a peatland, *Hydrological Processes*, 13, 1341–1359, 1999.
- Dugdale, S. J., Bergeron, N. E. and St-Hilaire, A.: Spatial distribution of thermal refuges analysed in relation to riverscape hydromorphology using airborne thermal infrared imagery, *Remote Sensing of Environment*, doi:10.1016/j.rse.2014.12.021, 2016.
- 650 Fraser, C. J. D., Roulet, N. T. and Lafleur, M.: Groundwater flow patterns in a large peatland, *Journal of Hydrology*, 246(1–4), 142–154, doi:10.1016/S0022-1694(01)00362-6, 2001.
- 655 Freeze, A. R.: A conceptual framework for assessing cumulative impacts on the hydrology of nontidal wetlands, *Environmental Management*, 12(5), 605–620, 1988.
- Freeze, R. A. and Witherspoon, P. A.: Theoretical analysis of regional groundwater flow- 2. Effect of water-table configuration and subsurface permeability variation, *Water Resources Research*, 3(2), 623–634, 1967.
- 660 Garrison, P. J. and Fitzgerald, S. A.: The role of shoreland development and commercial cranberry farming in a lake in Wisconsin , USA, *Journal of Paleolimnology*, 33(2), 169–188, 2005.
- 665



- Goto, S., Yamano, M. and Kinoshita, M.: Thermal response of sediment with vertical fluid flow to periodic temperature variation at the surface, *Journal of Geophysical Research B: Solid Earth*, 110(1), B01106, doi:10.1029/2004JB003419, 2005.
- 670 Grand-Clement, E., Anderson, K., Smith, D., Luscombe, D., Gatis, N., Ross, M. and Brazier, R. E.: Evaluating ecosystem goods and services after restoration of marginal upland peatlands in South-West England, edited by S. Wan, *Journal of Applied Ecology*, 50(2), 324–334, doi:10.1111/1365-2664.12039, 2013.
- 675 Hancock, R. N., Torgersen, C. E., Cherkauer, K. A., Gillespie, A. R., Tockner, K., Faux, R. N. and Tan, J.: Thermal infrared remote sensing of water temperature in riverine landscapes, in *Fluvial Remote Sensing for Science and Management*, pp. 85–113, John Wiley & Sons Inc., 2012.
- 680 Hare, D. K., Briggs, M. A., Rosenberry, D. O., Boutt, D. F. and Lane, J. W.: A comparison of thermal infrared to fiber-optic distributed temperature sensing for evaluation of groundwater discharge to surface water, *Journal of Hydrology*, 530, 153–166, doi:10.1016/j.jhydrol.2015.09.059, 2015.
- 685 Hatch, C. E., Fisher, A. T., Revenaugh, J. S., Constantz, J. and Ruehl, C.: Quantifying surface water-groundwater interactions using time series analysis of streambed thermal records: method development, *Water Resources Research*, 42(10), 2006.
- Holden, J.: Hydrological connectivity of soil pipes determined by ground-penetrating radar tracer detection, *Earth Surface Processes and Landforms*, 29(4), 437–442, doi:10.1002/esp.1039, 2004.
- 690 Irvine, D. J., Briggs, M. A., Lautz, L. K., Gordon, R. P., McKenzie, J. M. and Cartwright, I.: Using Diurnal Temperature Signals to Infer Vertical Groundwater-Surface Water Exchange., *Ground water*, doi:10.1111/gwat.12459, 2016.
- 695 Kettridge, N., Comas, X., Baird, A., Slater, L., Strack, M., Thompson, D., Jol, H. and Binley, A.: Ecohydrologically important subsurface structures in peatlands revealed by ground-penetrating radar and complex conductivity surveys, *Journal of Geophysical Research*, 113, 1–15, doi:10.1029/2008JG000787, 2008.



- 700 Knight, R.: Ground penetrating radar for environmental applications, *Annual Review of Earth and Planetary Sciences*, 29, 229–255, 2001.
- Koster, R. D., de Valpine, D. P. and Jouzel, J.: Continental water recycling and  $H_2^{18}O$  concentrations, *Geophysical Research Letters*, 20(20), 2215–2218, doi:10.1029/93GL01781, 1993.
- 705 Kruger, J., Kjaer, K. H. and Schomacker, A.: 7 dead-ice environments: a landsystems model for a debris-charged, stagnant lowland glacier margin, Kötlujökull, *Developments in Quaternary Science*, 13, 105–126, 2009.
- Kurylyk, B. L., MacQuarrie, K. T. B. and Voss, C. I.: Climate change impacts on the temperature and magnitude of groundwater discharge from shallow, unconfined aquifers, *Water Resources Research*, 50(4), 3253–3274, doi:10.1002/2013WR014588, 2014a.
- 710 Kurylyk, B. L., MacQuarrie, K. T. B., Linnansaari, T., Cunjak, R. a. and Curry, R. A.: Preserving, augmenting, and creating cold-water thermal refugia in rivers: concepts derived from research on the Miramichi River, New Brunswick (Canada), *Ecohydrology*, 8(6), 1095–1108, doi:10.1002/eco.1566, 2014b.
- Labaugh, J. W., Winter, T. C. and Rosenberry, D. O.: Hydrologic functions of prairie wetlands, *Great Plains Research*, 8, 17–37, 1998.
- 720 Lafleur, P. M., Moore, T. R., Roulet, N. T. and Frohling, S.: Ecosystem respiration in a cool Temperate bog depends on peat temperature but not water table, *Ecosystems*, 8(6), 619–629, doi:10.1007/s10021-003-0131-2, 2005.
- Larsen, L. G., Harvey, J. W. and Crimaldi, J. P.: A delicate balance: ecohydrological feedbacks governing landscape morphology in a lotic peatland, *Ecological Monographs*, 77(4), 591–614, 2007.
- 725 van Loon, A. H., Schot, P. P., Griffioen, J., Bierkens, M. F. P., Batelaan, O. and Wassen, M. J.: Throughflow as a determining factor for habitat contiguity in a near-natural fen, *Journal of Hydrology*, 379(1–2), 30–40, doi:10.1016/j.jhydrol.2009.09.041, 2009.





- Lowry, C. S., Walker, J. F., Hunt, R. J. and Anderson, M. P.: Identifying spatial variability of groundwater discharge in a wetland stream using a distributed temperature sensor, *Water Resources Research*, 43(10), 1–9, doi:10.1029/2007WR006145, 2007.
- 735 Lowry, C. S., Fratta, D. and Anderson, M. P.: Ground penetrating radar and spring formation in a groundwater dominated peat wetland, *Journal of Hydrology*, 373(1–2), 68–79, doi:10.1016/j.jhydrol.2009.04.023, 2009.
- Masterson, J. P., Carlson, C. S. and Walter, D. A.: Hydrogeology and simulation of groundwater flow in the Plymouth-Carver-Kingston-Duxbury aquifer system , southeastern Massachusetts, *Scientific Investigations Report 2009–5063*, 110p, 2009.
- 740 Masterson, J. P., Carlson, C. S. and Walter, D. A.: Hydrogeology and simulation of groundwater flow in the Plymouth-Carver-Kingston-Duxbury aquifer system , southeastern Massachusetts, *Scientific Investigations Report 2009–5063*, 110p, 2009.
- McBride, M. S. and Pfannkuch, H. O.: Distribution of seepage within lakebeds, *US Geological Survey Journal of Research*, 3(5), 505–512, 1975.
- 745 McBride, M. S. and Pfannkuch, H. O.: Distribution of seepage within lakebeds, *US Geological Survey Journal of Research*, 3(5), 505–512, 1975.
- McKenzie, J. M., Siegel, D. I., Rosenberry, D. O., Glaser, P. H. and Voss, C. I.: Heat transport in the Red Lake Bog , *Glacial Lake Agassiz Peatlands, Hydrological Processes*, 21, 369–378, doi:10.1002/hyp, 2007.
- Menberg, K., Blum, P., Kurylyk, B. L. and Bayer, P.: Observed groundwater temperature response to recent climate change, *Hydrology and Earth System Sciences*, 18(11), 4453–4466, doi:10.5194/hess-18-4453-2014, 2014.
- 750 Menberg, K., Blum, P., Kurylyk, B. L. and Bayer, P.: Observed groundwater temperature response to recent climate change, *Hydrology and Earth System Sciences*, 18(11), 4453–4466, doi:10.5194/hess-18-4453-2014, 2014.
- Newby, P. E., Killoran, P., Waldorf, M. R., Shuman, B. N., Webb, R. S. and Webb, T.: 14,000 years of sediment, vegetation, and water-level changes at the Makepeace Cedar swamp, southeastern Massachusetts, *Quaternary Research*, 53(3), 352–368, doi:10.1006/qres.1999.2120, 2000.
- 755 Newby, P. E., Killoran, P., Waldorf, M. R., Shuman, B. N., Webb, R. S. and Webb, T.: 14,000 years of sediment, vegetation, and water-level changes at the Makepeace Cedar swamp, southeastern Massachusetts, *Quaternary Research*, 53(3), 352–368, doi:10.1006/qres.1999.2120, 2000.
- Newby, P. E., Donnelly, J. P., Shuman, B. N. and MacDonald, D.: Evidence of centennial-scale drought from southeastern Massachusetts during the Pleistocene/Holocene transition, *Quaternary Science Reviews*, 28(17–18), 1675–1692, doi:10.1016/j.quascirev.2009.02.020, 2009.
- 760 Newby, P. E., Donnelly, J. P., Shuman, B. N. and MacDonald, D.: Evidence of centennial-scale drought from southeastern Massachusetts during the Pleistocene/Holocene transition, *Quaternary Science Reviews*, 28(17–18), 1675–1692, doi:10.1016/j.quascirev.2009.02.020, 2009.
- Parish, F., Sirin, A., Charman, D., Joosten, H., Minayeva, T. and Silviu, M.: Assessment on peatlands, biodiversity and climate change: main report., edited by L. Stringer, Global Environment Centre, Kuala Lumpur and Wetlands International. Wageningen., 2008.



- 765 Poulsen, J. R., Sebok, E., Duque, C., Tetzlaff, D. and Engesgaard, P. K.: Detecting groundwater discharge dynamics from point-to-catchment scale in a lowland stream: combining hydraulic and tracer methods, *Hydrology and Earth System Sciences*, 19(4), 1871–1886, doi:10.5194/hess-19-1871-2015, 2015.
- Price, J. S., Heathwaite, A. L. and Baird, A. J.: Hydrological processes in abandoned and restored peatlands : An overview of management approaches, *Wetlands Ecology and Management*, 11, 65–83, 2003.
- 770 Rau, G. C., Andersen, M. S., McCallum, A. M., Roshan, H. and Acworth, R. I.: Heat as a tracer to quantify water flow in near-surface sediments, *Earth-Science Reviews*, 129, 40–58, doi:10.1016/j.earscirev.2013.10.015, 2014.
- 775 Reeve, A. S., Evensen, R., Glaser, P. H., Siegel, D. I. and Rosenberry, D.: Flow path oscillations in transient ground-water simulations of large peatland systems, *Journal of Hydrology*, 316(1–4), 313–324, doi:10.1016/j.jhydrol.2005.05.005, 2006.
- 780 Rosenberry, D. O.: A seepage meter designed for use in flowing water, *Journal of Hydrology*, 359(1–2), 118–130, 2008.
- Rosenberry, D. O., Toran, L. and Nyquist, J. E.: Effect of surficial disturbance on exchange between groundwater and surface water in nearshore margins, *Water Resources Research*, 46(6), n/a-n/a, doi:10.1029/2009WR008755, 2010.
- 785 Rossi, P. M., Ala-aho, P., Ronkanen, A. and Kløve, B.: Groundwater–surface water interaction between an esker aquifer and a drained fen, *Journal of Hydrology*, 432–433, 52–60, doi:10.1016/j.jhydrol.2012.02.026, 2012.
- 790 Schmidt, C., Conant Jr., B., Bayer-Raich, M. and Schirmer, M.: Evaluation and field scale application of an analytical method to quantify groundwater discharge using mapped streambed temperatures, *Journal of Hydrology*, 347, 292–307, 2007.
- 795 Sebestyen, S. D. and Schneider, R. L.: Dynamic temporal patterns of nearshore seepage flux in a headwater Adirondack lake, *Journal of Hydrology*, 247, 137–150, 2001.



- Sebestyen, S. D. and Schneider, R. L.: Seepage patterns, pore water, and aquatic plants: hydrological and biogeochemical relationships in lakes, *Biogeochemistry*, 68(3), 383–409, 2004.
- 800
- Sebok, E., Duque, C., Kazmierczak, J., Engesgaard, P., Nilsson, B., Karan, S. and Frandsen, M.: High-resolution distributed temperature sensing to detect seasonal groundwater discharge into Lake Vaeng, Denmark, *Water Resources Research*, 49(9), 5355–5368, doi:10.1002/wrcr.20436, 2013.
- 805
- Sebok, E., Duque, C., Engesgaard, P. and Boegh, E.: Application of Distributed Temperature Sensing for coupled mapping of sedimentation processes and spatio-temporal variability of groundwater discharge in soft-bedded streams, *Hydrological Processes*, 29(15), 3408–3422, doi:10.1002/hyp.10455, 2015.
- Selker, J. S., Thevenaz, L., Huwald, H., Mallet, A., Luxemburg, W., de Giesen, N. V., Stejskal, M., Zeman, J., Westhoff, M., Parlange, M. B., Thévenaz, L. and Van De Giesen, N.: Distributed fiber-optic temperature sensing for hydrologic systems, *Water Resources Research*, 42(12), doi:doi:10.1029/2006WR005326, 2006.
- 810
- Shaw, S. B., Bonville, D. B. and Chandler, D. G.: Combining observations of channel network contraction and spatial discharge variation to inform spatial controls on baseflow in Birch Creek, Catskill Mountains, USA, *Journal of Hydrology: Regional Studies*, 12(June 2016), 1–12, doi:10.1016/j.ejrh.2017.03.003, 2017.
- 815
- Siegel, D. I., Reeve, A. S., Glaser, P. H. and Romanowicz, E. A.: Climate-driven flushing of pore water in peatlands, *Nature*, 374, 531–533, 1995.
- 820
- Silliman, S. E., Ramirez, J. and McCabe, R. L.: Quantifying Downflow through Creek Sediments Using Temperature Time-Series - One-Dimensional Solution Incorporating Measured Surface-Temperature, *Journal of Hydrology*, 167(1–4), 99–119, 1995.
- 825
- Slater, L. D. and Reeve, A.: Case history investigating peatland stratigraphy and hydrogeology using integrated electrical geophysics, *Geophysics*, 67(2), 365–378, 2002.
- Smart, R. P., Holden, J., Dinsmore, K. J., Baird, A. J., Billett, M. F., Chapman, P. J. and Grayson, R.: The dynamics of natural pipe hydrological behaviour in blanket peat, , doi:10.1002/hyp, 2012.
- 830
- Sophocleous, M.: Interactions between groundwater and surface water: the state of the science, *Hydrogeology Journal*, 10(1), 52–67, 2002.



- 835 Stallman, R. W.: Steady one-dimensional fluid flow in a semi-infinite porous medium with sinusoidal surface temperature, *Journal of Geophysical Research*, 70(12), 2821–2827, doi:Cited By (since 1996) 106Export Date 4 April 2012, 1965.
- Turcotte, D. L. and Schubert, G.: *Geodynamics: applications of continuum physics to geological problems*, John Wiley & Sons, New York, 1982.
- 840 Tyler, S. W., Selker, J. S., Hausner, M. B., Hatch, C. E., Torgersen, T., Thodal, C. E. and Schladow, S. G.: Environmental temperature sensing using Raman spectra DTS fiber-optic methods, *Water Resources Research*, 45, doi:doi:10.1029/2008WR007052, 2009.
- Vandenbohede, a., de Louw, P. G. B. and Doornbal, P. J.: Characterizing preferential groundwater discharge through boils using temperature, *Journal of Hydrology*, 510, 372–384, doi:10.1016/j.jhydrol.2014.01.006, 2014.
- 850 Verberk, W. C. E. P., Bilton, D. T., Calosi, P. and Spicer, J. I.: Oxygen supply in aquatic ectotherms: Partial pressure and solubility together explain biodiversity and size patterns, *Ecology*, 92(8), 1565–1572, 2011.
- Wallage, Z. E. and Holden, J.: Near-surface macropore flow and saturated hydraulic conductivity in drained and restored blanket peatlands, *Soil Use and Management*, 27(2), 247–254, doi:10.1111/j.1475-2743.2011.00336.x, 2011.
- 855 Watters, J. R. and Stanley, E. H.: Stream channels in peatlands: The role of biological processes in controlling channel form, *Geomorphology*, 89(1–2), 97–110, doi:10.1016/j.geomorph.2006.07.015, 2007.
- 860 Winter, T. C.: Effects of water-table configuration on seepage through lake beds, *Limnology and Oceanography*, 26(5), 925–934, doi:10.4319/lo.1981.26.5.0925, 1981.
- Winter, T. C.: The concept of hydrologic landscapes, *Journal of American Water Resources Association*, 37(2), 335–349, 2001.



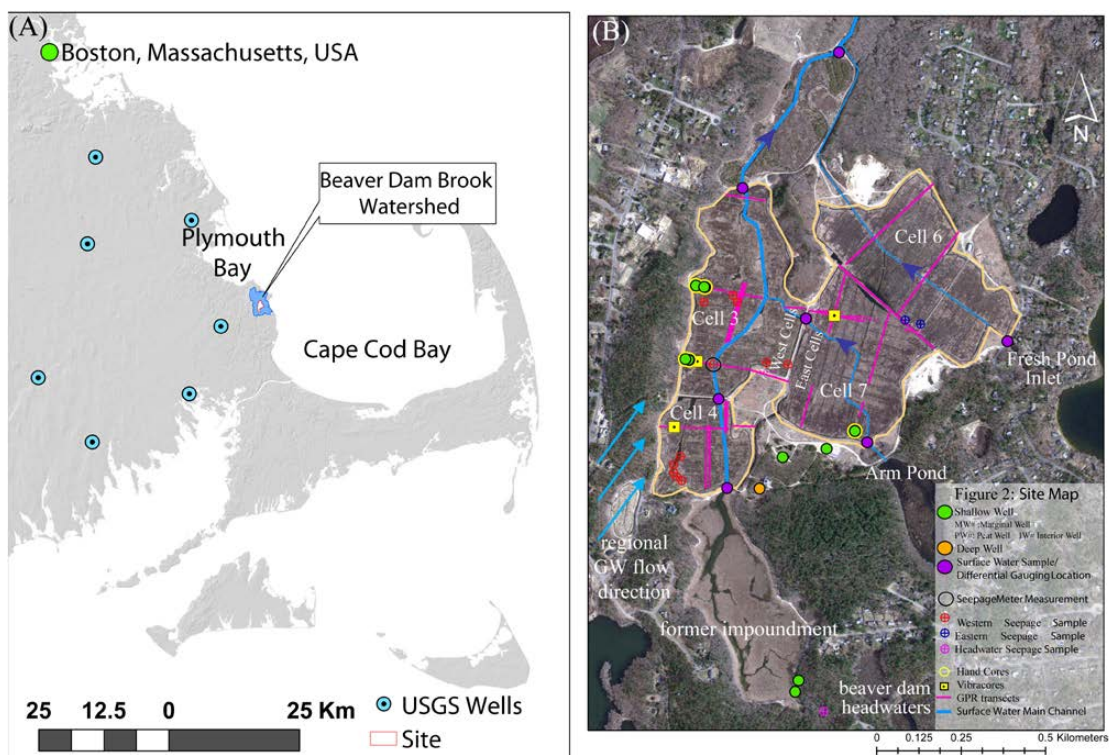
- 865 Winter, T. C., Harvey, J. W., Franke, O. L. and Alley, W. M.: Ground water and surface water; a single resource, U. S. Geological Survey Circular, , 79, 1998.



USGS Well ID	$\delta^{18}\text{O}$	$\delta^2\text{H}$	Latitude (WGS 84)	Longitude (WGS 84)
MA-PWW 494, Plymouth	-6.15	-37.38	41.8713889	-70.6586111
MA-EBW 30, East Bridgewater	-8.07	-46.33	42.0155556	-70.9658333
MA-WFW 51 Wareham	-6.83	-37.45	41.7550000	-70.7325000
MA-D4W 80 Duxbury	-8.13	-47.42	42.0547222	-70.7247222
MA-XGW 2, Weymouth	-8.55	-50.33	42.1650000	-70.9458333
MA-NGW 116, New Bedford	-7.55	-43.42	41.6736111	-70.9577778
MA-F3W 23, Freetown	-7.86	-44.02	41.7847222	-71.0813889

870

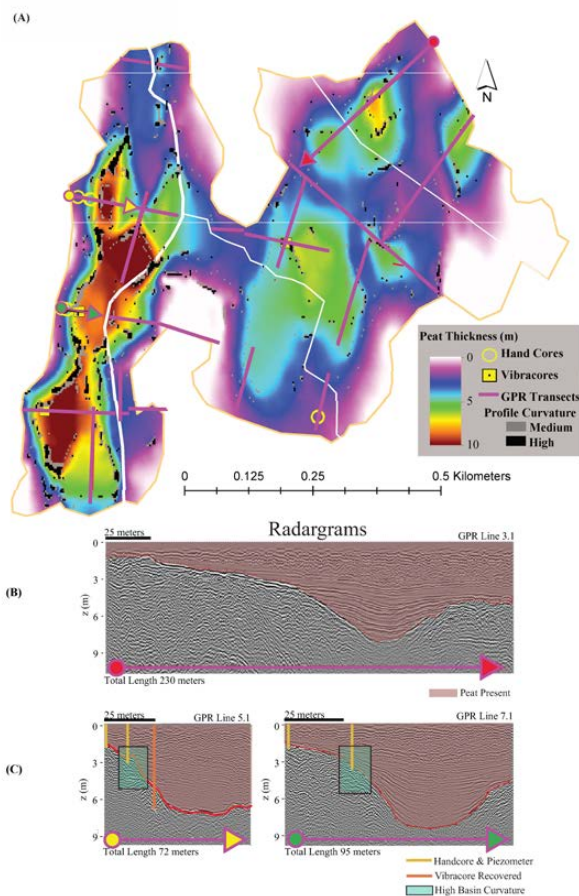
**Table 1:** USGS groundwater wells  $\delta^2\text{H-H}_2\text{O}$ ,  $\delta^{18}\text{O-H}_2\text{O}$  isotopic data used to establish the regional groundwater trend.



875

Figure 1: a) Site map of the Tidmarsh Farms regional peatland showing the study area and watershed boundary; Plymouth County, Massachusetts, and PCKD USGS wells used for regional groundwater isotopic data (Table 1). b) Detail of the Tidmarsh Farms study site showing the major waterways and flow direction in blue, site groundwater wells, isotopic sample locations, and GPR transects. Beaver Dam Brook flows north into Plymouth Bay.

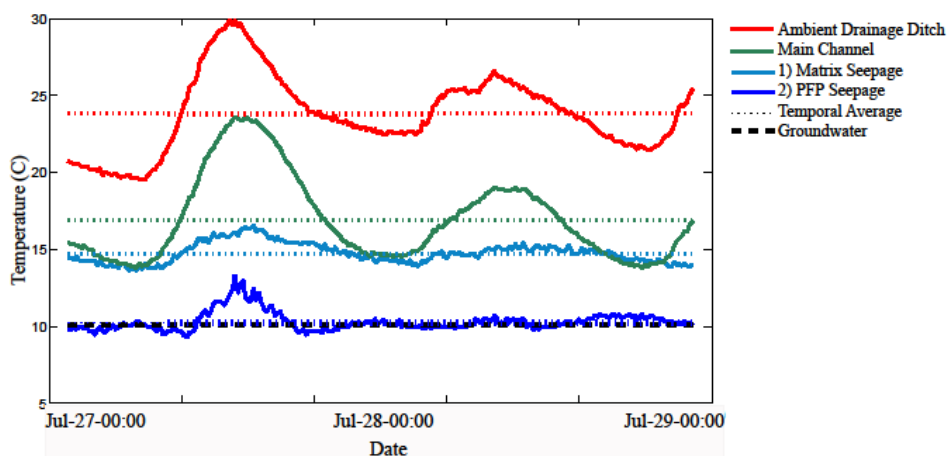
880



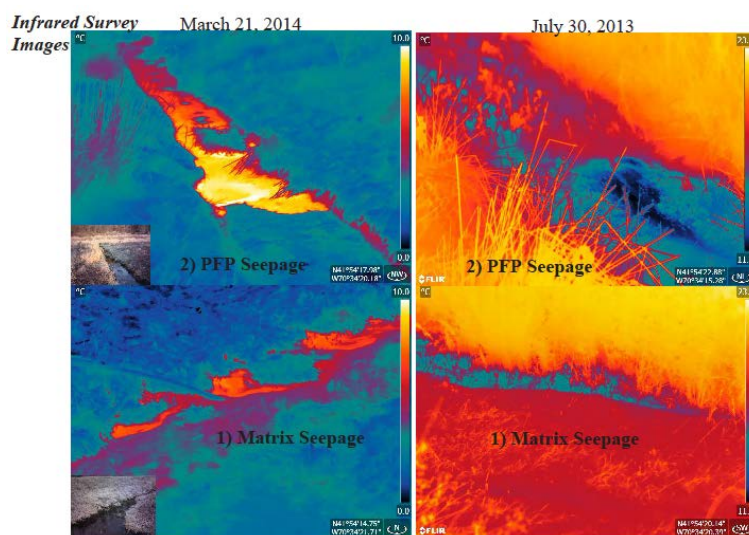
885 **Figure 2:** a) Map of total peat thickness beneath Tidmarsh Farms based on GPR data. GPR data collected along  
linear transects show here (pink lines) were interpolated and contoured to show the 3D surface. Zones of  
medium and high curvature (the 2nd derivative of the thickness) of the peat-sand interface are shown as grey  
and black pixels, respectively. b) Three example cross sectional profiles, or radargrams, illustrate a distinct  
reflector at the basal peat-sand contact. Peat is shaded red, and sediment core samples used to constrain the  
GPR velocity data are also shown as yellow (hand cores) and orange lines (vibracore). High curvature is  
highlighted in green.

890





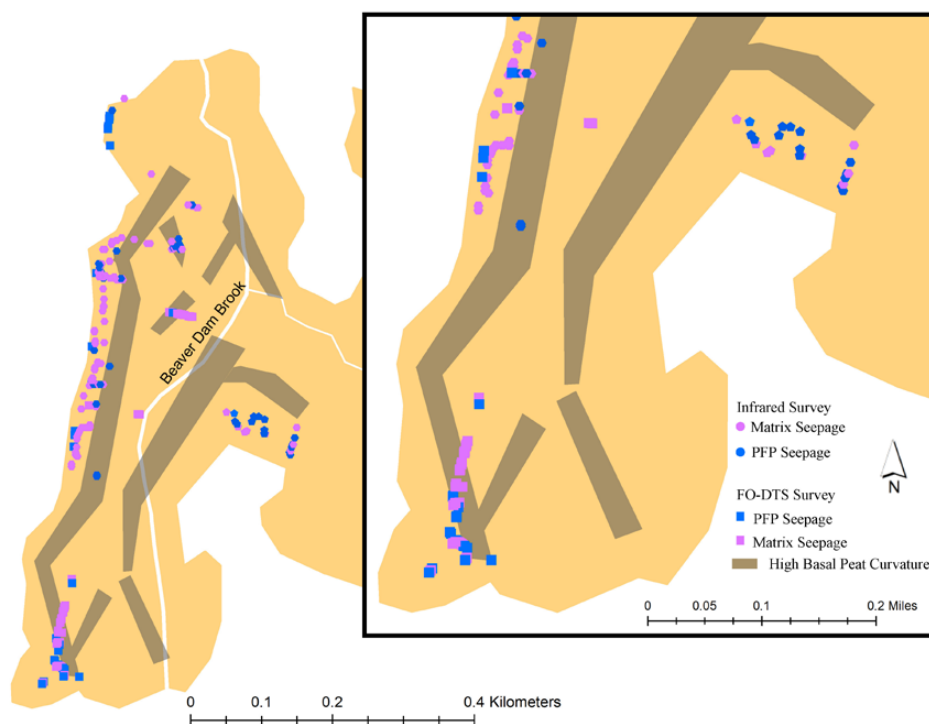
895 **Figure 3:** Fiber-optic Distributed Temperature Sensing (FO-DTS) temperature time series from four 1-meter segments of cable to illustrate the characteristic thermal signatures at Tidmarsh Farms. The greatest amplitude and variability occurs in the drainage ditches with little flow and significant solar heating (red), followed by the main channel of Beaver Dam Brook (green). Two seepage types, matrix (type 1) seepage, with very low variability (low standard deviation) over time and a mean temperature a few degrees higher than groundwater (light blue) and preferential flow path (type 2) seepage with a mean temperature nearly equal to groundwater (dark blue) are also plotted over 2.5 days.



900

905

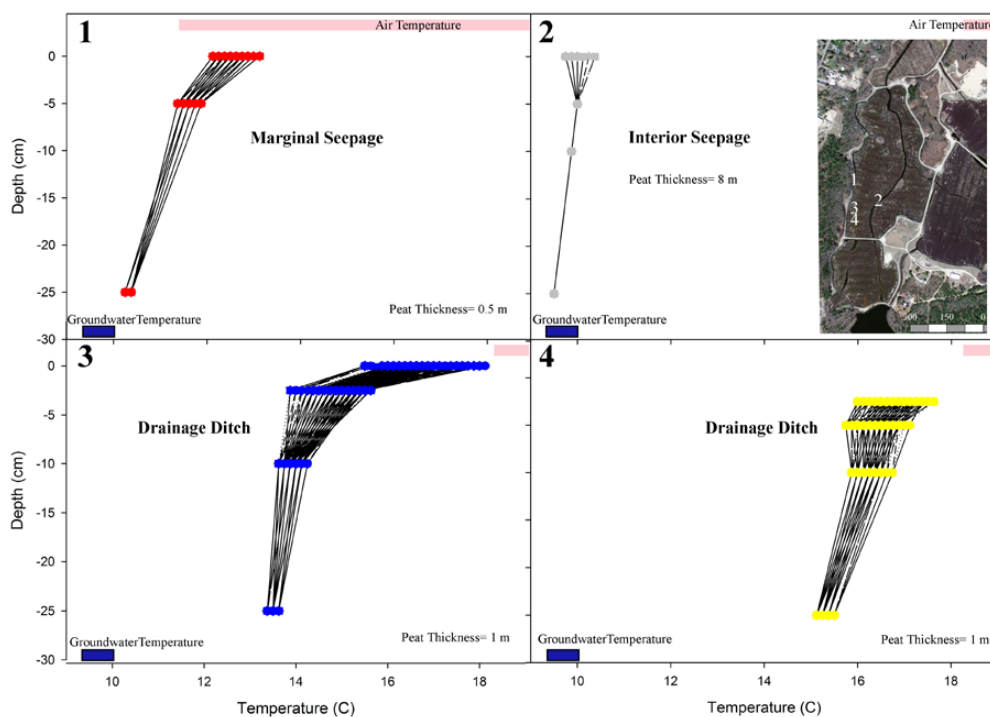
Figure 4: Thermal infrared (TIR) images recorded in July 30-31, 2013 (Summer) and March 21, 2014 (Winter) at Tidmarsh Farms. Visible light images are shown in the bottom left of March images, but not July, as these surveys were conducted at night to limit issues associated with reflectance. TIR images illustrate the two types of seepage in both seasons: type 1 preferential flow path seepage that is characterized by discrete discharge points very close to groundwater temperature with high-flux, and type 2 matrix seeps that are diffuse, 3-5 °C warmer or cooler than groundwater and lower flux.



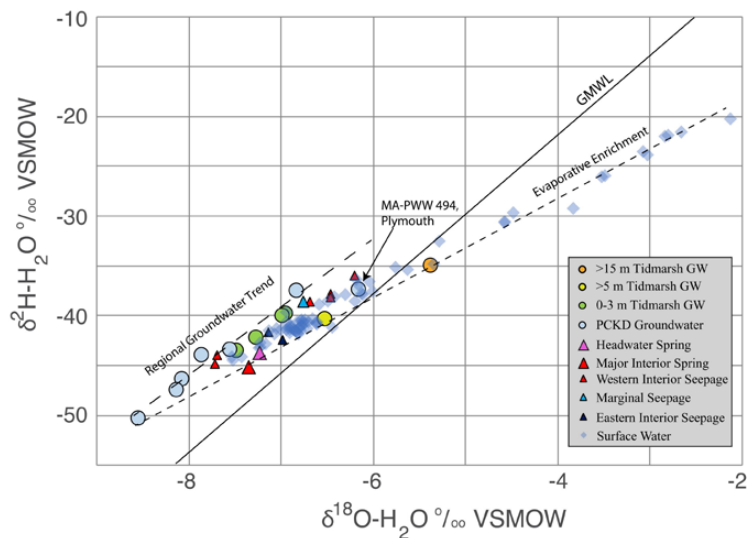
910 **Figure 5: Map of seepage at Tidmarsh Farms determined with fiber-optic distributed temperature sensing (FO-**  
**DTS, squares) and thermal infrared (TIR) surveys (circles). Background shaded region(s) match the bounded**  
**area from Figure 1B, and darker background shading delineates zones of high curvature (the 2nd derivative of**  
**the thickness) of the peat-sand interface (Fig. 2). For both methods, light purple to pink symbols indicate matrix**  
**(type 1) seepage, and dark blue indicates locations of PFP (type 2) seepage. From FO-DTS data, a location was**  
**tagged as seepage if the standard deviation was less than 1.5 and the temperature was less than 15 °C for matrix**  
915 **and less than or equal to 11 °C for PFP seepage. From TIR surveys, seepage was distinguished by temperatures**  
**of 9-11 °C for interior seepage, and 11-15 °C for matrix seepage.**



920 **Figure 6:** Thermal infrared (TIR) image from March 21, 2014 at Tidmarsh Farms illustrating PFP (type 2) seepage. Many macropores are observed in both the infrared (slightly smaller) and the visual image. These seeps are located in the middle of cell 3 (Fig. 1B), where peat is ~3m thick and dramatically thinning.



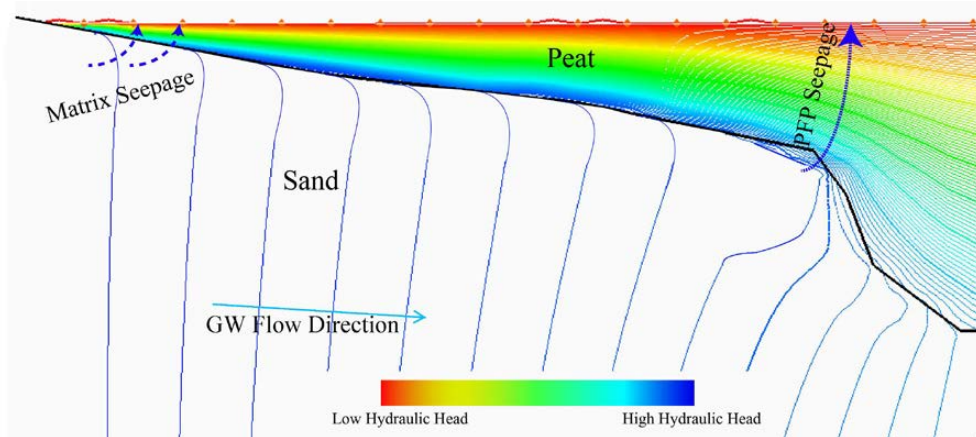
925 **Figure 7: Temperature profiles vs. depth at Tidmarsh Farms recorded in July 30-31, 2013. For each profile, the range of air temperatures and groundwater (GW) temperatures are shown as pink (air) and dark blue (groundwater(GW)) bands. At locations 1 and 2, (profiles 1 and 2) show the influence of upwelling groundwater; expressed as type 1 preferential flow path (PFP) seepage (profile 2) and type 2 matrix seepage (profile 1). The concave shape of temperature-depth profiles 3 and 4 is also indicative of upwelling seepage.**



930

**Figure 8:** Plot of the stable isotopes  $\delta^2\text{H}$  and  $\delta^{18}\text{O}$  from the Tidmarsh Farms area surface water, groundwater, shallow well, and seep sources. The regional groundwater trend line was derived from samples from relatively shallow, regional USGS wells (blue dots, shaded grey region), consistent with a relatively humid climate at the site.

935



940

**Figure 9: Conceptual model illustrating the mechanism for development of matrix (type 1) seepage and preferential flow path (PFP) or interior (type 2) seepage, shown as dashed lines. The thick black line represents the peat-sand interface, and outlines a typical basin shape. Solid colored lines show contours of equal hydraulic potential. Often associated with locations of high basin curvature, strong vertical gradients drive focused, higher flux seepage through pre-existing weaknesses in the peat matrix.**